example, sedimentary basins, geothermal systems, island arcs, oceanic ridges, and contact aureoles). Various hydrous minerals (clays, zeolites, micas, talc, serpentine, chlorite, epidotes, and amphiboles) form under these conditions as primary or alteration minerals, and their isotopic compositions have been used to infer the source of fluids or the temperature of mineral formation (isotope geothermometer). Many mineral water D/H fractionation factors in the literature, which were usually determined at a constant, high pressure (typically ≥100 MPa), are rather insensitive to temperature (*6*). However, pressure changes alone can shift mineral water D/H fractionation factors as shown for the system brucite water (Fig. 3). Thus, if not taken into account, pressure variations could lead to large errors in the isotopic composition of the fluid calculated to be in equilibrium with the mineral (≥10 per mil in δD) or in the estimated temperature of mineral formation (≥100°C in calculated temperatures).

References and Notes

1. H. W. Joy and W. F. Libby, *J. Chem. Phys.* **33**, 1276 (1960); R. N. Clayton, in *Thermodynamics of Minerals and Melts*, R. C. Newton, A. Navrotsky, B. J. Wood, Eds. (Springer-Verlag, New York), pp. 85–109 (1981); S. D. Hamann, R. M. Shaw, J. Lusk, B. D. Batts, *Aust. J. Chem.* **37**, 1979 (1984); Z. D. Sharp, E. J. Essene, J. R. Smyth, *Contrib. Mineral. Petrol.* **112**, 358 (1992); P. Gillet, P. McMillan, J. Schott, J. Badro, A. Grzechnik, *Geochim. Cosmochim. Acta* **60**, 3471 (1996); V. B. Polyakov, *Geochim. Cosmochim. Acta* **62**, 3077 (1998).
2. V. B. Polyakov and N. N. Kharlashina, *Geochim. Cosmochim. Acta* **58**, 4739 (1994).
3. T. C. Hoering, *Carnegie Inst. Washington Year Book* **60**, 201 (1961); R. N. Clayton, J. R. Goldsmith, K. J. Karel, T. K. Mayeda, R. C. Newton, *Geochim. Cosmochim. Acta* **39**, 1197 (1975); Y. Matsuhisa, J. R. Goldsmith, R. N. Clayton, *Geochim. Cosmochim. Acta* **43**, 1131 (1979); A. Matthews, J. R. Goldsmith, R. N. Clayton, *Geochim. Cosmochim. Acta* **47**, 631 (1983); A. Matthews, J. R. Goldsmith, R. N. Clayton, *Geol. Soc. Am. Bull.* **94**, 396 (1983); M. R. Palmer, D. London, G. B. Morgan, IV, H. A. Babb, *Chem. Geol.* **101**, 123 (1992); T. Driesner, thesis, Eidgenössische Technische Hochschule, Zurich, Switzerland (1996).
4. W. Kohl, H. A. Lindner, E. U. Franck, *Ber. Bunsenges. Phys. Chem.* **95**, 1586 (1991); J. D. Frantz, J. Dubessy, B. Mysen, *Chem. Geol.* **106**, 9 (1993).
5. T. Driesner, *Science* **277**, 791 (1997).
6. T. W. Vennemann and J. R. O'Neil, *Geochim. Cosmochim. Acta* **60**, 2437 (1996), and references therein.
7. S. D. Mineev and V. A. Grinenko, *J. Conf. Abst.* **1**, 404 (1996).
8. J. V. Walther, *Geochim. Cosmochim. Acta* **50**, 733 (1986); T. B. Bai and A. F. Koster van Groos, *Am. Mineral.* **83**, 205 (1998); K. Shinoda and N. Aikawa, *Phys. Chem. Minerals* **25**, 197 (1998); P. Gillet, R. J. Hemley, P. F. McMillan, in *Ultrahigh-Pressure Mineralogy*, R. J. Hemley, Ed. (Reviews in Mineralogy 37, American Mineralogical Society, 1998), pp. 525–590.
9. Typically, 10 to 25 mg of brucite and 25 to 300 mg of water were sealed in gold capsules. Three or four gold capsules, identical except for hydrogen isotope composition of water within the capsule, were loaded into an autoclave, cold-seal apparatus, or piston cylinder depending on the pressure-temperature conditions of interest. Temperature and pressure were controlled within ±2°C and ±1 MPa, respectively, except for low-pressure (15 to 25 MPa) experiments, for which pressure was calculated from the volume of the vessel and pressure-temperature-volume properties of pure water to an error of ±0.2 to 1 MPa. In a piston cylinder experiment at 800 MPa, a pressure uncertainty is ±20 MPa. At the end of experiments, the vessels were quenched to <50°C within 5 to 30 min, and the gold capsules were weighed to check for leakage. The brucite run products were washed with deionized water and dried. After drying in vacuum overnight at 150°C, water was extracted from brucite by heating to 900°C for an hour in a vacuum. The water extracted was converted to H_2 by passing over hot uranium metal at 750°C [J. Bigeleisen, M. L. Perlman, H. C. Prosser, *Anal. Chem.* **24**, 1356 (1952)].
10. D. A. Northrop and R. N. Clayton, *J. Geol.* **74**, 174 (1966).
11. T. Suzuoki and S. Epstein, *Geochim. Cosmochim. Acta* **40**, 1229 (1976).
12. L. Haar, J. S. Gallagher, G. S. Kell. *NBS/NRC Steam Tables* (Taylor & Francis, Washington, DC, 1984).
13. H. Satake and S. Matsuo, *Contrib. Mineral. Petrol.* **86**, 19 (1984).
14. P. J. Saccocia, J. S. Seewald, W. C. Shanks III, *Geochim. Cosmochim. Acta* **62**, 485 (1998); B.-L. Xu and Y.-F. Zheng, *Geochim. Cosmochim. Acta* **63**, 2009 (1999).
15. V. B. Polyakov, personal communication (1999).
16. D. B. Wenner and H. P. Taylor Jr., *Am. J. Sci.* **273**, 207 (1973); H. Sakai and M. Tsusumi, *Earth Planet Sci. Lett.* **40**, 231 (1978); C. M. Graham, R. S. Harmon, S. M. F. Sheppard, *Am. Mineral.* **69**, 128 (1984); D. Blamart, M. Pichavant, S. M. F. Sheppard, *C.R. Acad. Sci. Paris* **308**, 39 (1989); G. Jibao and Q. Yaqian, *Geochim. Cosmochim. Acta* **61**, 4679 (1997); T. Chacko, L. R. Riciputi, D. R. Cole, J. Horita, *Geochim. Cosmochim. Acta* 63, 1 (1999).
17. R. N. Clayton, J. R. Goldsmith, T. K. Mayeda, *Geochim. Cosmochim. Acta* **53**, 725 (1989); J. M. Rosenbaum, *Geochim. Cosmochim. Acta* **61**, 4993 (1997).

18. Sponsored by the U.S. Department of Energy Geoscience Program, under contract DE-AC05-96OR22464 with Oak Ridge National Laboratory, managed by Lockheed Martin Energy Research Corp., and by a postdoctoral fellowship of the Swiss National Science Foundation. We thank D. Wesolowski, T. Labotka, T. Seward, V. Polyakov, and P. Ulmer for their comments and support.

2 July 1999; accepted 19 October 1999

A Laboratory Model for Convection in Earth's Core Driven by a Thermally Heterogeneous Mantle

Ikuro Sumita* and Peter Olson

Thermal convection experiments in a rapidly rotating hemispherical shell suggest a model in which the convection in Earth's liquid outer core is controlled by a thermally heterogeneous mantle. Experiments show that heterogeneous boundary heating induces an eastward flow in the core, which, at a sufficiently large magnitude, develops into a large-scale spiral with a sharp front. The front separates the warm and cold regions in the core and includes a narrow jet flowing from the core-mantle boundary to the inner-core boundary. The existence of this front in the core may explain the Pacific quiet zone in the secular variation of the geomagnetic field and the longitudinally heterogeneous structure of the solid inner core.

The temperature profile in Earth's outer core is estimated to be nearly adiabatic (*1*) as a consequence of its highly turbulent state. The total heat flux from the core to the mantle is estimated to be comparable to (within a factor of 2) the heat conducted down the core adiabat (*1, 2*). These conditions lead to an unusual thermal regime in which the turbulent convective heat transfer amounts to less than one-half of the total heat transfer from the core. The situation is further complicated by a heterogeneous heat-flow boundary condition due to the large-scale pattern of mantle convection. As a consequence, the convective part of the heat transfer in the core is likely to exhibit extremely large lateral variations, perhaps of more than an order of magnitude (*3*).

The importance of a thermally heterogeneous core-mantle boundary (CMB) for convection in the core has been recognized (*4*). Theoretical studies have investigated the flow driven by boundary heterogeneity, but mostly in the cases in which the heat-flux variation is relatively small (*5*). These studies have shown that, under some conditions, the convective pattern in the core can be locked to the CMB heterogeneity. In the core, we expect a generally convective state modulated by a large lateral variation in convective heat flux. In our study, we modeled this regime using laboratory experiments in a rapidly rotating spherical shell (*6*). Such experiments realize conditions closer to those of Earth by an order of magnitude, as compared to numerical models (*7*), and also include the fine-scale structures that tend to be smoothed out in numerical models.

A hemispherical shell (Fig. 1) was filled with water and rotated at 206 rotations per minute, providing an Ekman number of $E = 4.7 \times 10^{-6}$. Radial gravity was simulated by the combined effects of Earth's gravity and centrifugal acceleration. The outer copper sphere, the model CMB, was maintained at room temperature. The inner copper sphere, the inner-core boundary (ICB), was maintained be-

Department of Earth and Planetary Sciences, Johns Hopkins University, Baltimore, MD 21218, USA.

*To whom correspondence should be addressed. E-mail: sumita@ekman.eps.jhu.edu

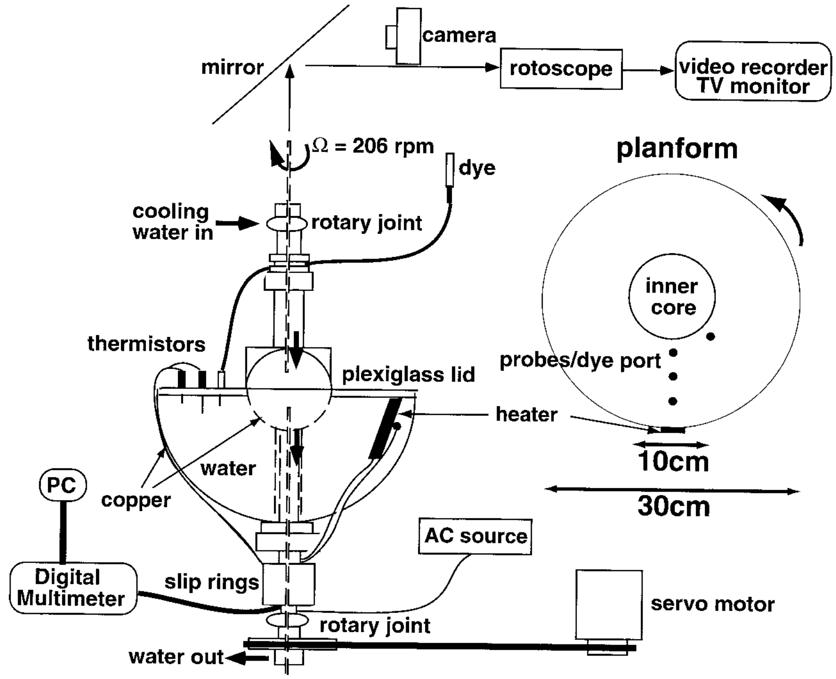

Fig. 1. Diagram of the experimental apparatus.

low room temperature. Thermal heterogeneity was imposed by attaching a heat-flux-regulated, thermally insulated rectangular heater at the CMB, covering a latitudinal and longitudinal rectangle of 0° to 48° and 0° to 9.7°, respectively, which is 2.3% of the CMB area (*8*). This patch modeled the effect of an anomalously cold region in Earth's lower mantle, where heat flow from the core to the mantle is large. The heat-flux variation in the experiments modeled the heat-flux variation in the core in excess of that conducted down the adiabat. The total heat flux at the ICB was measured by the temperature rise of the water circulating in and out of the inner core. We recorded the temporal and spatial variations of the pattern, flow velocity, and temperature.

With a homogeneous thermal boundary condition, convection in the fully developed regime consists of nearly two-dimensional turbulence, with meandering plumes originating from the ICB and CMB (*6*). The mean zonal flow is westward, and the convective pattern drifts westward with this flow. We refer to this as the basic convective state.

Figure 2 shows how this basic state is modified by boundary heterogeneity for $19 < Ra/Ra_c < 52$ (*Ra* is Rayleigh number, Ra_c is critical Rayleigh number), $E = 4.7 \times 10^{-6}$, and for lateral variation of heat flux at the CMB up to ~100 times its mean value. When the peak heat flux at the CMB is less than ~35 times its mean, the mean convective structure remains unaltered from the basic state (Fig. 2A). However, there is a localized eastward flow adjacent to the heterogeneity. Temperature in the fluid measured by thermistor probes indicates a higher temperature and a larger fluctuation to the east of the heterogeneity. This eastward phase shift is consistent with some of the previous theoretical studies (*5*). As the heat flux is increased, the anomalous flow extends toward the ICB, and temperature fluctuation changes from the predominance of spikes with negative anomaly to positive anomaly, indicating that the flow is increasingly driven by warm plumes. Because the anomalous flow is confined near the heater at the CMB, we refer to this regime as local locking.

A much different regime appears when the peak heat flux at the CMB exceeds its mean by ~35 times, featuring a large spiraling structure to the east of the heterogeneity (Fig. 2B). Dye streaks show that the flow is eastward near the heterogeneity, with a narrow radially inward flowing jet along the spiral structure (Fig. 2C). These flows are two-dimensional curtains aligned along the rotational axis, implying an essentially geostrophic balance. The spiral and the jet divide the warm region to the west from the cold region to the east, preventing mixing between them. Measurements show a trend of an eastward increase of temperature approaching the jet followed by a sharp drop in temperature across the jet. The spiral remains fixed in relation to the heterogeneity, forming a stationary front. Visual observations and temperature measurements show that the ICB (CMB) side of the front is dominated by cold (warm) plumes because the stationary front blocks the radial motion of the warm (cold) plumes. As the magnitude of heating is increased, the front extends eastward. Heat-flux measurements at the ICB show that, at $Ra/Ra_c \simeq 30$, ~40% of the heat anomaly is advected radially across the shell, and the rest is advected laterally along the CMB. Because the basic state is replaced by a front

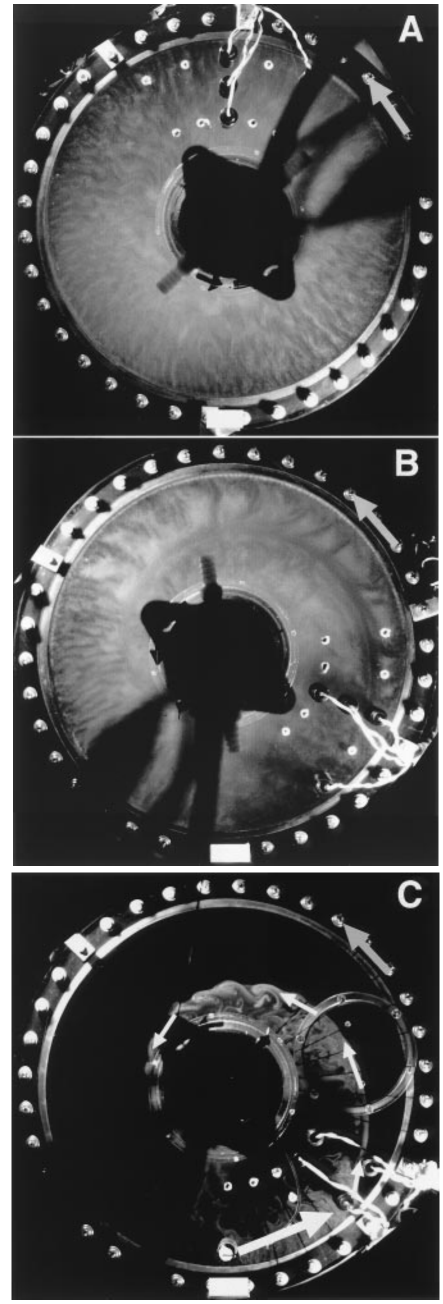

Fig. 2. Equatorial planform of rotating hemispherical shell convection with anomalous heat flux at CMB (heater, white rectangle) at $E = 4.7 \times 10^{-6}$, visualized by (**A** and **B**) flakes and (**C**) fluorescent dye. Rotation is anticlockwise. (A) Local locking regime at a supercritical Rayleigh number $Ra/Ra_c = 26$ ($\Delta T = 6.9$°C). The peak CMB heat flux is 20 times its mean ($\Delta T_{cmb} = 1.5$°C). (B) Global locking at $Ra/Ra_c = 24$ ($\Delta T = 6.2$°C). The peak CMB heat flux is 95 times its mean ($\Delta T_{cmb} = 12.8$°C). The spiraling stationary front originates from the CMB 50° east of the heater. (C) Global locking at $Ra/Ra_c = 26$ ($\Delta T = 6.7$°C). The peak CMB heat flux is 69 times its mean ($\Delta T_{cmb} = 7.5$°C). White dye was injected adjacent to the heater. White arrows indicate induced flows [eastward flow (broad arrow) and a narrow jet along the front (fine arrows)]. The velocities of the eastward flow and the jet are $\sim 1.5 \times 10^{-3}$ and $\sim 5.2 \times 10^{-3}$ m/s, respectively.

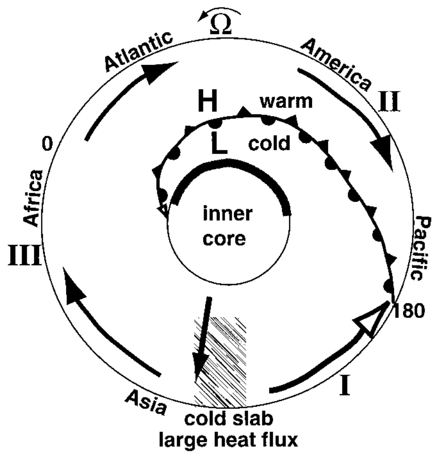

Fig. 3. Schematic diagram of the equatorial planform of Earth's core as seen from the North Pole, showing a CMB patch with high heat flux (hatched area) producing global locking of the core flow pattern. Rotation is counterclockwise. The temperature variations and the direction of the gravity is appropriate for Earth's core and is opposite to the experiments. The numbers indicate longitude. Black (white) headed arrows indicate warm (cold) large-scale flows. Dominant zonal and radial flows in the equatorial region of the three sectors are as follows: I, eastward and downwelling; II, westward and downwelling; and III, westward and upwelling. The front with a jet separates I and II. H and L indicate the high- and low-pressure regions, respectively. The shaded region at the ICB is the inferred region of fast solidification.

extending across the shell, we refer to this regime as global locking.

A balance between Coriolis acceleration and thermal buoyancy in a columnar flow model (*9*) shows that an eastward decrease (increase) of the CMB temperature results in a downwelling (upwelling). This generates a cyclonic circulation, which develops into an eastward spiral for large heat-flux heterogeneity. Because the heterogeneity induces a warm eastward flow in contrast to the cold westward flow, a convergence of flows occurs, forming a front, and the pressure gradient associated with the density difference across the front drives the geostrophic jet (*10*). We estimate the lateral variation of convective heat flux needed for global locking to be comparable to a factor of 35 (*11*). Estimates of the lateral variation of heat flux at the CMB, with the heat conducted down the adiabat removed, indicate that local and global styles of locking are possible in Earth's core (*3*).

On the basis of the experiments, we propose the following model for the flow in Earth's core under global locking (Fig. 3). We expect a similar large-scale structure to exist in the core because of the heat-flux heterogeneity imposed by the mantle. We also expect fine-scale structures, although their spatial and temporal scales may be modified by the magnetic field. We assume that the flow is basically geostrophic, consistent with the presence of geomagnetic features that can be attributed to columnar flow (*12*). For simplicity, we only consider anomalous CMB heat flow from the prominent seismically fast region near CMB beneath east Asia (*13*). If there are two antipodal heterogeneities of the same strength, the experiments show that the eastward extent of the front is restricted. The observed absence of the westward drifting of the geomagnetic flux patches in the Pacific (*12*) is similar to the global locking regime for two reasons: (i) the front blocks the upwellings from the inner core and may inhibit the westward drifting flux patches from forming (*14*) and (ii) the eastward flow and the front blocks the mean westward flow. The directions of azimuthal flow in Fig. 3 agree with outer core flow models obtained from geomagnetic secular variation using tangentially geostrophic approximation (*15*), which is consistent with the columnar nature of flows. We estimate the width and the velocity of the jet in the core as 10 km and 7×10^{-3} m/s, respectively, assuming a temperature difference across the front of $\sim 10^{-4}$°C (*10, 16*). This shows that a localized flow can exist in the core, faster than the mean azimuthal flow of $\sim 10^{-4}$ m/s, inferred from the geomagnetic westward drift. Global locking is also expected to result in a hemispherical dichotomy in the growth of the inner core because of the differences in the heat flow at the ICB across the front. The model predicts a rapid inner core crystallization on the cold side of the front, leading to higher porosity and a larger growth-induced anisotropy in the inner core (*17*). This agrees with seismological evidence revealing slow *P*-wave velocity and large anisotropy in the western hemisphere of the inner core (*18*). The orientation of the inner core seismic structure in relation to the CMB heterogeneity agrees with the eastward phase shift we observed in the experiments.

References and Notes

1. F. D. Stacey, *Physics of the Earth* (Brookfield, Brisbane, Australia ed. 3, 1992), pp. 330–337.
2. B. A. Buffett, H. E. Huppert, J. R. Lister, A. W. Woods, *J. Geophys. Res.* **101**, 7989 (1996).
3. The total heat flux at the top of the convective region of the core, q_{CMB}, is the sum of the conductive heat flux along the adiabat q_{ad} and the convective heat flux q_{conv}, $q_{CMB} = q_{ad} + q_{conv}$. q_{ad} can be assumed to be laterally uniform. In contrast, q_{conv} is variable; here, we assume it has a high and a low value, q_{conv}^{high} and q_{conv}^{low}, respectively. We suppose q_{conv}^{high} is found over some fractional area f of the CMB. Then, the mean heat flow at the CMB can be expressed as $\bar{q}_{CMB} = q_{ad} + f q_{conv}^{high} + (1 - f) q_{conv}^{low}$. We define the lateral variation of total heat flux as $A = (q_{ad} + q_{conv}^{high})/(q_{ad} + q_{conv}^{low})$ and the mean Nusselt number by $Nu = \bar{q}_{CMB}/q_{ad}$. Then, the lateral variation of convective heat flux is given by $B = q_{conv}^{high}/q_{conv}^{low} = [ANu - 1 - f(A - 1)]/[Nu - 1 - f(A - 1)]$. Estimates for Earth are $A \leq 10$ (from mantle convection calculations) and $Nu = 1.1$ [$\bar{q}_{CMB} = 20$ mW/m^2 and $q_{ad} = 18$ mW/m^2 (*2*)]. Assuming $f = 2.3\%$ (the same as the experiments), for $A = 1.5$, we obtain $B \simeq 7$, and for $A = 4$, we obtain $B \simeq 80$. Hence, a small lateral variation in q_{CMB} implies a large lateral variation in q_{conv} in the core.
4. G. M. Jones, *J. Geophys. Res.* **82**, 1703 (1977); J. Bloxham and D. Gubbins, *Nature* **325**, 511 (1987).
5. K. Zhang and D. Gubbins, *Geophys. J. Int.* **108**, 247 (1992); *J. Fluid Mech.* **250**, 209 (1993); *Phys. Fluids* **8**, 1141 (1996); S. Yoshida and Y. Hamano, *J. Geomagn. Geoelectr.* **45**, 1497 (1993); Z.-P. Sun, G. Schubert, G. A. Glatzmaier, *Geophys. Astrophys. Fluid Dyn.* **75**, 199 (1994); P. Olson and G. A. Glatzmaier, *Philos. Trans. R. Soc. London Ser. A* **354**, 1413 (1996); G. R. Sarson, C. A. Jones, A. W. Longbottom, *Phys. Earth Planet. Inter.* **101**, 13 (1997); G. A. Glatzmaier and P. H. Roberts, *Contemp. Phys.* **38**, 269 (1997).
6. I. Sumita and P. Olson, *Phys. Earth Planet. Inter.*, in press, and references therein.
7. Thermal convection in rotating systems is characterized by three dimensionless numbers: the Ekman number $E = \nu/\Omega D^2$, the Rayleigh number $Ra = \alpha g \Delta T D^3/\kappa\nu$, and the Prandtl number $Pr = \nu/\kappa$, where ν is kinematic viscosity, Ω is rotation rate, D is shell thickness, α is thermal expansivity, g is gravity, ΔT is superadiabatic temperature difference, and κ is thermal diffusivity. For core, $E \simeq 10^{-16}$, and $Pr = 0.015$. Assuming $\Delta T \geq 4 \times 10^{-6}$ K, we obtain $Ra/Ra_c \geq 75$ ($Ra_c \sim 10^{19}$ for nonmagnetic thermal convection). The Reynolds number is $Re = VD/\nu \sim 10^8$. For the experiments, $E = 4.7 \times 10^{-6}$, $Ra/Ra_c \leq 52$ ($Ra_c = 1.8 \times 10^7$), $Pr = 7$, and Re is of the order of 10^2.
8. The heater imposes a fixed total heat flux on the fluid. The perturbed temperature at the outer boundary has a Gaussian profile, with a longitudinal half-width of ~30°. Longitudinal temperature variation at the boundary ΔT_{cmb} is defined as the temperature difference between the heater and its antipode. Ra is calculated with ΔT between inner and outer boundaries at the antipode of the heater. Thermal boundary condition is constant heat flux at the heater and becomes isothermal at far field. The heat flux was increased stepwise from the basic state.
9. P. Cardin and P. Olson, *Phys. Earth Planet. Inter.* **82**, 235 (1994).
10. Thermally induced flow is estimated by $V_{th} \sim \alpha g \Delta T_{cmb}/2\Omega$. The jet velocity V_{jet} and its width δ are estimated from the balance between vortex generation, stretching, and advection (*9*) as $V_{jet} \simeq (\alpha g \Delta T_{front})^{2/3} (D/\Omega)^{1/3}$ and $\delta \simeq (\alpha g \Delta T_{front})^{1/3} (D/\Omega)^{2/3}$, where ΔT_{front} is the temperature difference across the front. For Fig. 2C, $\Delta T_{cmb} \leq 7.5$°C, and $\Delta T_{front} \simeq 1.5$°C; we obtain $V_{th} \leq 2.6 \times 10^{-3}$ m/s, $V_{jet} \simeq 7 \times 10^{-3}$ m/s, and $\delta \simeq 3$ mm, which agree with the measurements (Fig. 2C).
11. In the experiments, conduction down the radial temperature gradient contributes ~10% of the total heat transfer, and its lateral variation is negligible in comparison to lateral variation of convective heat flux.
12. D. Gubbins and J. Bloxham, *Nature* **325**, 509 (1987).
13. R. D. van der Hilst and H. Kárason, *Science* **283**, 1885 (1999), and references therein.
14. J. Bloxham, *Geophys. J. R. Astron. Soc.* **87**, 669 (1986).
15. For example, J. Bloxham, *J. Geophys. Res.* **97**, 19565 (1992).
16. ΔT_{front} scales as $\sim q_{conv}/\rho C_p V_{th}$, where q_{conv} is the convective heat flux at the heterogeneity, ρ is the density, and C_p is the heat capacity. For the core, assuming $q_{conv} \simeq 50$ mW/m^2 and $V_{th} \simeq 10^{-4}$ m/s, we obtain $\Delta T_{front} \simeq 10^{-4}$°C. A similar hemispherical temperature variation of $\simeq 10^{-3}$°C was obtained from geomagnetic secular variation, revealing a cold Pacific [J. Bloxham and A. Jackson *Geophys. Res. Lett.* **17**, 1997 (1990)].
17. I. Sumita, S. Yoshida, M. Kumazawa, Y. Hamano, *Geophys. J. Int.* **124**, 502 (1996); S. Yoshida, I. Sumita, M. Kumazawa, *J. Geophys. Res.* **101**, 28085 (1996).
18. S. Kaneshima, *Geophys. Res. Lett.* **23**, 3075 (1996); S. Tanaka and H. Hamaguchi, *J. Geophys. Res.* **102**, 2925 (1997); K. C. Creager, *J. Geophys. Res.* **104**, 23127 (1999). A degree one seismic heterogeneity was obtained at the top of the outer core S. Tanaka and H. Hamaguchi, in *Dynamics of Earth's Deep Interior and Earth Rotation*, vol. 72 of *Geophysical Monograph Series*, J.-L. Le Mouël, D. E. Smylie, T. Herring, Eds. (American Geophysical Union, Washington, DC, 1993), pp. 127–134.

19. Supported by Research Fellowships of the Japan Society for the Promotion of Science for Young Scientists (I.S.) and the Geophysics Program of NSF.

28 June 1999; accepted 18 October 1999